35th Annual International Conference of the IEEE EMBS
Osaka, Japan, 3 - 7 July, 2013

Segmentation of Hepatic Tumor from Abdominal CT Data Using An Improved Support Vector Machine Framework *

Jiayin Zhou, *Member, IEEE*, Weimin Huang, *Member, IEEE*, Wei Xiong, *Member, IEEE*, Wenyu Chen, and Sudhakar K. Venkatesh

Abstract— **An improved support vector machine (SVM) framework has been developed to segment hepatic tumor from CT data. By this method, the one-class SVM (OSVM) and two-class SVM (TSVM) are connected seamlessly by a boosting tool, to tackle the tumor segmentation via both offline and online learning. An initial tumor region was first pre-segmented by an OSVM classifier. Then the boosting tool was employed to automatically generate the negative (non-tumor) samples, according to certain criteria. The pre-segmented initial tumor region and the non-tumor samples generated were used to train a TSVM) classifier. By the trained TSVM classifier, the final tumor lesion was segmented out. Tested on 16 sets of CT abdominal scans, quantitative results suggested that the developed method achieved significantly higher segmentation accuracy than the OSVM and TSVM classifiers.**

I. Introduction

Hepatic tumors, especially hepatocellular carcinoma and hepatic metastases, are serious threatens to human health. Contrast-enhanced computed tomography (CT) is widely used for the detection, diagnosis and management of hepatic tumor. Tumor bulk is an important measure of the severity of diseases and tumor volumetry is used for cancer management and treatment response assessment [1-2]. In addition, accurate lesion localization is a necessary step to plan some diagnostic and therapeutic procedures such biopsy, ablation, radiotherapy, etc. Manual contouring of tumor margin is a tedious procedure and prone to considerable intra- and inter-observer variability. Thus, automated and robust tumor segmentation and quantification is increasingly receiving attention from the research community.

Hepatic tumors always show different image properties from the surrounding tissues/structures in CT images. Typically the identification and extraction of abnormal regions from an image region-of-interest (ROI) can be treated as a two-class classification for the separation of tumor and non-tumor classes. There were some studies on the segmentation of hepatic tumor by the support vector machine (SVM), a supervised learning-based method for binary and multi-class classifications [3]. Zhou et al developed a semi-automatic scheme for the segmentation of 3D hepatic tumors from CT images. The main technique is a two-class SVM (TSVM) classifier cum a propagational learning strategy for automated sampling, learning and further voxel classification among neighboring slices [4]. For the semi-automatic segmentation method reported by Freiman et al, it first classifies the liver voxels into tumor and healthy tissue with a TSVM engine from which a new set of high-quality seeds is generated. Over the 3D images, these seeds then conduct the propagation procedure, which is controlled by an energy function describing the affinity constraints, to obtain the final tumor region [5]. In the work of Zhang et al, CT volume is partitioned into a large number of catchment basins under watershed transform. Then a SVM classifier is trained by user-selected seed points to extract tumors from liver parenchyma, while the corresponding feature vector is computed based upon each small region produced by watershed transform [6]. The common process in these work is to online learn the actual data distributions of target (tumor) and non-target (non-tumor) data by sampling, then train SVM classifiers and extract the target data, with the assistance of linear/non-linear kernel mapping.

It is clear that the classification performance of SVM is influenced by training samples as SVM is based on supervised learning. These "representative" training samples, which well reflect the distribution properties of the whole data, are needed in order to learn the actual distribution properties of data explored. However, the selection of "representative" training samples may not be easy, especially in selecting non-target samples. In tumor segmentation case, it is probably not difficult to pick up tumor samples from images, however the manual selection of "representative" non-tumor samples must be careful because non-tumor data, which usually include highly diverse tissue types, occupy the majority portion in both image and feature spaces in most cases. In fact, the arbitrariness in selecting non-tumor samples may cause considerable intra-/inter-operator variability in segmentation results. An alternative is to use the one-class SVM (OSVM) [7], a variant of SVM. An OSVM classifier can extract tumor region by learning data distribution from user-selected tumor samples only and non-tumor samples are unnecessary. However, this method may achieve low true positive rates or high false positive rates for heterogeneous tumors with blurry boundary, due to the low discriminative power in OSVM-based data recognition.

We developed an improved SVM framework which complementarily combines OSVM and TSVM by a boosting tool for hepatic tumor segmentation. In the rest of the paper, we describe the details of the method to elaborate how this framework works for tumor segmentation and benchmark its performance with other methods using clinical CT data.

*Research supported by a research grant (JCOAG03-FG05_2009) from the Joint Council Office, A*STAR, Singapore.

J. Zhou, W. Huang, W. Xiong and W. Chen are with the Institute for Infocomm Research, Agency for Science Technology and Research, Singapore 138632, Singapore (corresponding author: J. Zhou; phone: +65 6408-2497; e-mail: jzhou@ i2r.a-star.edu.sg).

S. K. Venkatesh is with the Department of Radiology, Mayo Clinic, Rochester, MN 55905 USA.

II. METHOD

A. Overview

The workflow of the proposed method is shown in Fig. 1. An initial tumor region is first pre-segmented by an OSVM classifier. Then the negative (non-tumor) samples are automatically generated by a boosting tool, according to certain criteria. The pre-segmented initial tumor region, which is considered as the positive samples, and the negative samples generated are used to train a TSVM classifier to segment out the final tumor lesion. In this scheme, the good discrimination capability of TSVM is utilized to be the main segmentation tool, while the good recognition capability of OSVM is employed to be the guidance tool. The TSVM and the OSVM are connected by a boosting tool through the automatic generation of negative samples.

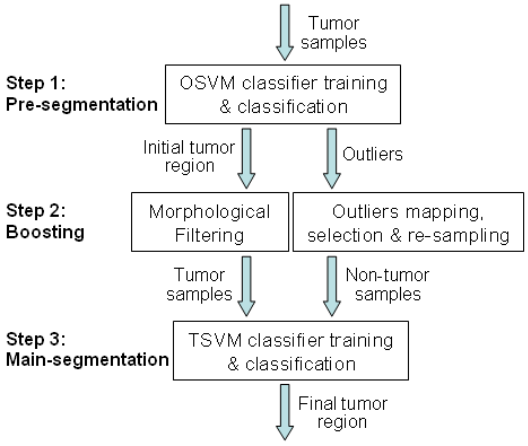

Figure 1. The flowchart of the proposed SVM segmentation framework.

B. Algorithm Details

Step 1 — Pre-segmentation: First an OSVM classifier was trained by user-selected tumor samples. Then the trained OSVC was used to extract the initial tumor region from a rectangular ROI, as shown in Fig. 2. For the OSVM, the only available training data are from one class, i.e., the target class (here is the tumor class) and there is no information about the other class, i.e., the outlier class. The OSVM will define a boundary around the target class, such that it accepts as many of the targets as possible and excluding the outliers as many as possible. By a proper kernel mapping M that maps the data $\boldsymbol{X}$ to a higher dimensional feature space, a hypersphere can be sought to enclose the mapped target data with a smallest radius R and center C.

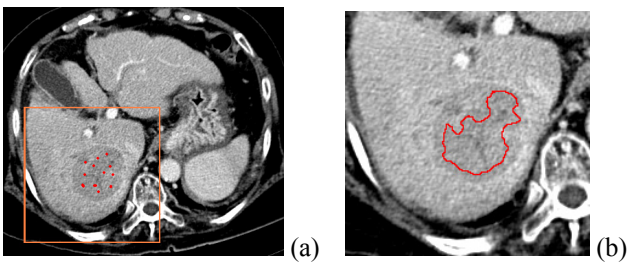

Figure 2. (a) The tumor samples selected and the ROI; (b) initially segmented tumor region by the OSVM classifier.

Step 2 — Boosting: In many cases, the initial tumor region extracted from Step 1 is not satisfying. The majority of the extracted tumor region is inside the actual tumor region and its boundary has some distance to the actual tumor boundary. Hence another data classification procedure utilizing the discrimination capability of TSVM follows up. Requiring both tumor and non-tumor samples, training a TSVM classifier is equivalent to finding an optimal hyperplane in a way that minimizes the error on the training dataset and maximize the perpendicular distance between the decision boundary and the closest data points in the two classes [3]. Here the initial tumor region extracted at Step 1 using the OSVM classifier was used as the positive training samples. The negative training samples came from the "outliers" recognized by the OSVM at Step 1. For the OSVM at Step 1, data recognized as the target (tumor) were enclosed by the optimally constructed hypersphere in the higher dimensional feature space whereas data which were not recognized as the target scattered at the region outside the hypersphere. These outliers include non-tumor voxles, tumor voxels but unrecognized, and marginal voxels. The further an outlier is to the hypersphere, the less similar it is to the tumor class and the less likelihood it belongs to tumor class. Outliers which have high likelihood to be non-tumor voxels can be selected out for the BSVM training, according to certain selection criteria. In this study, suppose the radius of optimal hypersphere is R, those data which scattered at the region outside the concentric hypersphere (C, mR [$m>1$]) were mapped backward into the image space, as shown in Fig. 3. They were used as the negative training samples after re-sampling, to equalize the numbers of samples from the positive. In Fig. 3, solid spots inside the hypersphere (C, R) in feature space were mapped into image space as the positive samples (red region), and the hollow spots outside the hypersphere (C, mR) were mapped into image space and re-sampled as the negative samples (green scatters).

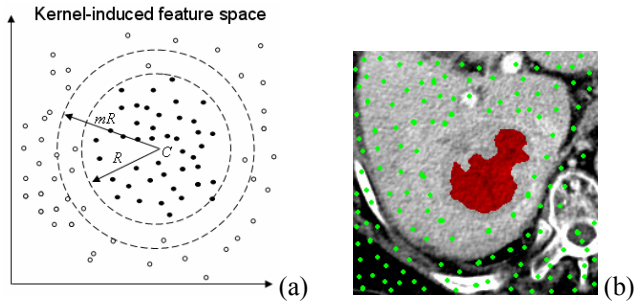

Figure 3. The illustrator of mapping data spots from the higher-dimensional feature space (a) to the image space (b).

Step 3 — Main-segmentation: A TSVM classifier was trained using the positive and negative samples generated in Step 2. Then the trained classifier was applied into the ROI again to segment the tumor lesion by binary classification, as shown in Fig. 4. By such a heuristic process in Step 2, more positives samples can be picked up for the training of the TSVM classifier and the most important, an equal number of negative samples, which are very important for TSVM training, can be automatically generated. No user selection operation for negative samples is required.

Figure 4. Tumor region segmented in Step 3.

C. Determination of Parameter 'm'

According to experience, most of these true tumor voxels unrecognized by OSVM classifier locate at the marginal area of the tumor which has the fuzzy transition to the marginal non-tumor area. Therefore before the backward-mapping, as shown in Fig. 4, parameter *m* (*m*>1) was used to control the filtering of these possible marginal tumor voxels, preventing them from being the possible non-tumor samples. Of course an excessively large *m* will filter out many true non-tumor voxels as well, hence the value of *m* needs to be tuned carefully such that the resultant new outliers include non-tumor voxels at a higher portion (ideal value, 100%) and tumor voxels at a lower portion (ideal value, 0). For this study, the proper value of *m* was determined in an off-line experiment manner by the greedy method:

For one CT slice with expert-labeled tumor ground truth (*GT*), an OSVM classifier can be trained using operator-selected tumor samples to segment out the tumor lesion. Given different *m* values, different sets of new outliers (non-tumor voxels) were obtained by the filtering of hypersphere (*C*, *mR*) in the high-dimensional feature space. Assume that in the ROI, voxel number of tumor *GT* is K_T, voxel number of non-tumor region is $K_{N\text{-}T}$, voxel number from new outliers but belonging to tumor *RS* is L_T, voxel number from new outliers but belonging to non-tumor region is $L_{N\text{-}T}$, and let $Co = L_{N-T}/K_{N-T} - L_T/K_T$. A higher value of *Co* means a more appropriate value of *m*, under the assumption that with a good *m*, the resultant outliers should have a high portion of real non-tumor voxels and a low portion of real tumor voxels. Given individual *m* value variable from 1 to *n* (*n*>*1*) with a small internal, an appropriate *m* value can be determined by experiment using a batch of training data with traced tumor *GTs*.

III. Implementation and Experiment

Voxel density indicated by Hounsfield Unit (HU) and its derivates are the most common low-level image features used for CT data analysis. In DICOM format, the voxel density is of 12-bit integer in data depth, but CT data will be converted into images of 8-bit integer in data depth for display and interpretation purposes, with different window level and width settings (window level, window width) to highlight different anatomic structures. The standard abdominal window is set at (50, 350), by which the organs and structures in abdominal region can be well visualized. To examine the hepatic region, especially to detect hepatic tumors, a window width of 350 is still too wide so that some tumors may be overlooked due to the close image intensities shown in this window. In practice, radiologists often use a narrower window width to observe hepatic region. Here a customized 'liver window' [8] for CT data rescaling was adopted: The liver window has a window center equal to the density of liver parenchyma and a window width of 180. In the implementation, each 12-bit CT data volume was rescaled into 2 set of 8-bit images using (1) the standard abdominal window (50, 350) and (2) the customized liver window (density of liver parenchyma, 180), where the density of liver parenchyma were obtained by online sample selection. The corresponding image intensities from the 2 sets of images form a concurrent feature vector (I_{AW}, I_{LW}) to be used as the low-level image feature for the segmentation. In addition, the Gaussian radius basis function (RBF) $K(\mathbf{x},\mathbf{y}) = \exp(-\|\mathbf{x}-\mathbf{y}\|^2/2\sigma^2)$ was adopted as the learning kernel in this study. The degree of similarity of two data points can be reflected by the kernel width parameter σ, hence a proper σ gives a trade-off between the tight separating margin and the potential over-fitting. An online learning scheme was adopted in this study hence for each slice to segment, the value of σ was set as the standard deviation calculated from the learning samples of tumor class.

The experimental data include abdominal CT scans from 20 patients acquired on one 64-detector CT scanner, using a standard four-phase contrast-enhanced imaging protocol with slice thickness of 1-3 mm, matrix of 512 × 512 pixels and in-plane resolution of 0.6-0.9 mm. An experienced abdominal radiologist identified and manually traced out 32 isolated hepatic tumors. By using the greedy method described in Section II.C and data from 16 tumors with the corresponding *GT*, an *m* value of 1.25 was determined with cross validation. The remaining 16 tumors were used for algorithm testing.

The proposed method was benchmarked with the OSVM and TSVM classifiers. Segmented tumors were compared with *GT* by spatial voxel matching. Two quantitative measures, volumetric overlap error (*VOE*, %) and average symmetric surface distance (*ASSD*, mm), were calculated to quantitatively assess the similarity between the computerized and manually defined tumors [9]. A *VOE* value is 0 is for a perfect segmentation and a value of 100% means that there is no overlap at all between segmentation and *GT*. *ASSD* tells us how much on average the two surfaces differ and the value is 0 for a perfect segmentation. In addition, inter-operator variance (*IV*) [10] was used to estimate the inter-operator reliability of each method for segmentation attempts conducted by different users. A lower *IV* value means the better inter-operator consistency.

IV. Results

CT slices bearing 16 hepatic tumors from 9 data sets were tested in the experiment. Fig. 5 shows the images of two cases of liver lesions, including the original images, the manually traced *GT*s, and the corresponding segmentation results using OSVM classifier, TSVM classifier and the proposed one. For Fig. 5 Row I, an arterial phase image shows a heterogeneous hypo-dense lesion with blurry margin to the surrounding liver parenchyma. The result from the proposed method is better than those from OSVM and TSVM classifier, though all the three methods miss the peri-tumoral artery. This hyper-density mass is on the right side of

the tumor and is generally included into the entire tumor volume. In Row II, a portal venous phase image shows a large hypo-dense hepatic lesion and the proposed one demonstrated improved capability in identifying peripheral tumor regions with fuzzy transition to the healthy liver parenchyma, compared to the other two which failed. Eight consecutive CT slices from one scan and the corresponding segmentation results using the proposed method are demonstrated in Fig. 6. The quantitative validations at voxel level for segmentation results using the three methods are summarized in Table I. For the proposed method, *VOE* and *ASSD* obtained are significantly lower than those obtained by using OSVM and TSVM (p<0.05, Kruskal-Wallis test). The OSVM obtained the best result of *IV* and the *IV* obtained by the proposed method is slightly higher, however no significant difference is shown. The *IVs* from OSVM and the proposed method are significantly lower than that from TSVM (p<0.05, Kruskal-Wallis test). Both quantitative and visual results obtained showed that compared to OSVM and TSVM, the developed algorithm achieved better results for hepatic tumor segmentation.

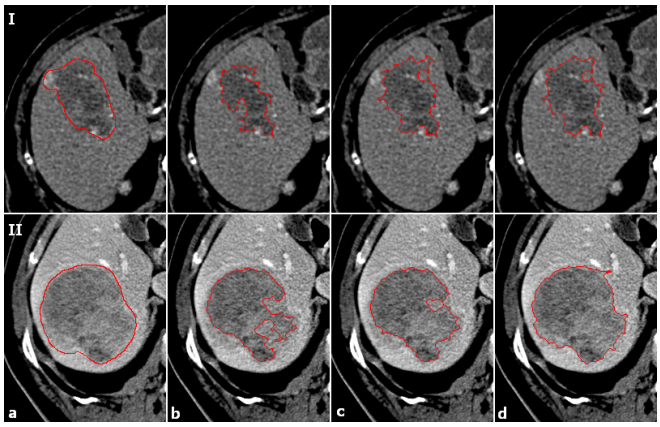

Figure 5. Hepatic tumor segmentation results. Row I: an example in arterial phase, Row II: another example in portal venous phase; Column a: original images with *GT* traced; Column b: result from the OSVM; Column c: result from the TSVM; Column d: result obtained by the proposed method.

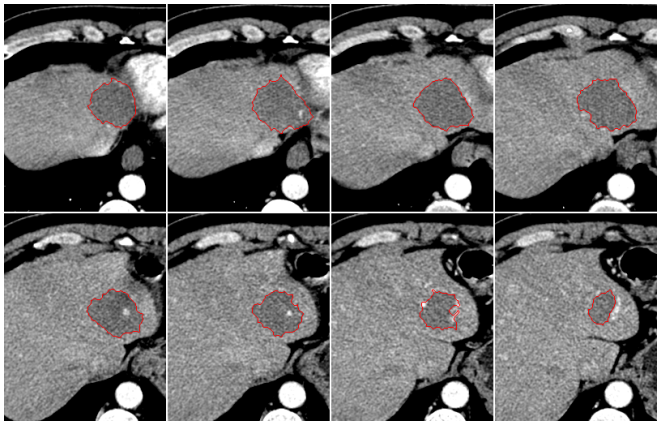

Figure 6. Segmentation results using the proposed method on 8 consecutive CT slices from one scan.

V. Conclusion

A three-step image segmentation method using an improved SVM framework has been developed to segment hepatic tumor from CT images. In this method, the OSVM and the TSVM were seamlessly connected in series by a boosting tool, for the automated generation and optimization of negative training samples. Implicitly the advantages of OSVM and TSVM were kept and some of their demerits were suppressed, leading to the better classification performance for tumor region. Experimental results suggested that the developed method achieved better segmentation accuracy than OSVM and TSVM, and better inter-operator consistency than TSVM.

TABLE I. QUANTITATIVE EVALUATION OF HEPATIC TUMOR SEGMENTATION

	VOE (%)			***ASSD*** (mm)			***IV*** (%)		
	O*	T*	P*	O*	T*	P*	O*	T*	P*
Min	18.2	23.9	17.3	1.3	0.8	0.6	11.3	19.0	14.3
Max	50.1	43.7	35.4	4.7	2.7	2.1	26.4	33.2	27.8
Mean	39.4	32.1	27.0	2.3	1.8	1.4	17.6	25.9	19.6
STD	9.4	6.4	6.7	1.0	0.7	0.6	4.6	5.0	4.8

VOE: volumetric overlap errors; *ASSD*: average symmetric surface distance; *IV*: inter-operator variance; O*, T* and P* stand for OSVM classifier, TSVM classifier and the proposed method, respectively.

References

[1] L. Van Hoe, E. Van Cutsem, I. Vergote, A. L. Baert, E. Bellon, P. Dupont, and G. Marchal, "Size quantification of liver metastases in patients undergoing cancer treatment: reproducibility of one-, two-, and three-dimensional measurements determined with spiral CT," *Radiology*, vol. 202, no. 3, pp. 671–675, Mar. 1997.

[2] S. R. Prasad, K. S. Jhaveri, S. Saini, P. F. Hahn, E. F. Halpern, and J. E. Sumner, "CT tumor measurement for therapeutic response assessment: comparison of unidimensional, bidimensional, and volumetric techniques—Initial observations," *Radiology*, vol. 225, no. 2, pp. 416-419, Nov. 2002.

[3] B. Schölkopf, and A. J. Smola, *Learning with Kernels Support Vector Machines: Regularization, Optimization and Beyond*. Cambridge, MA: MIT Press, 2002.

[4] J. Zhou, W. Xiong, Q. Tian, Y. Qi, J. Liu, W. L. Leow, H. Thazin, S. K. Venkatesh, and S. C. Wang, "Semi-automatic segmentation of 3D liver tumors from CT scans using voxel classification and propagational learning," In *Proc. MICCAI Workshop on 3D Segmentation in the Clinic: A Grand Challenge II*, New York, 2008.

[5] M. Freiman, O. Cooper, D. Lischinski, and L. Joskowicz, "Liver tumors segmentation from CTA images using voxels classification and affinity constraint propagation," *Int. J. Comput. Assist. Radiol. Surg.*, vol. 6, no. 2, pp. 247-255, Mar. 2011.

[6] X. Zhang; J. Tian; D. Xiang; X. Li, and K. Deng, "Interactive liver tumor segmentation from ct scans using support vector classification with watershed," In *Proc. 33rd IEEE-EMBC*, Boston, MA, 2011, pp. 6005-6008.

[7] D. M. Tax, and R. P. Duin, "Support vector data description," *Mach. Learn.*, vol. 54, vol. 1, pp. 45-66, Jan. 2004.

[8] W. W. Mayo-Smith, H. Gupta, M. S. Ridlen, J. M. Brody, N. C. Clements, and J. J. Cronan, "Detecting hepatic lesions: the added utility of CT liver window settings," *Radiology*, vol. 210, no. 3, pp. 601-604, Mar. 1999.

[9] M. Gerig, and M. V. Chakos, "A new validation tool for assessing and improving 3D object segmentation," In *Proc. 4th MICCAI*, Utrecht, The Netherlands, 2001, pp. 516-523.

[10] V. F. Chong, J. Y. Zhou, J. B. Khoo, J. Huang, and T. K. Lim, "Nasopharyngeal carcinoma tumor volume measurement," *Radiology*, vol. 231, no. 3, pp. 914-921, Jun. 2004.